

Nanoscale

Accepted Manuscript



This is an *Accepted Manuscript*, which has been through the Royal Society of Chemistry peer review process and has been accepted for publication.

Accepted Manuscripts are published online shortly after acceptance, before technical editing, formatting and proof reading. Using this free service, authors can make their results available to the community, in citable form, before we publish the edited article. We will replace this *Accepted Manuscript* with the edited and formatted *Advance Article* as soon as it is available.

You can find more information about *Accepted Manuscripts* in the [Information for Authors](#).

Please note that technical editing may introduce minor changes to the text and/or graphics, which may alter content. The journal's standard [Terms & Conditions](#) and the [Ethical guidelines](#) still apply. In no event shall the Royal Society of Chemistry be held responsible for any errors or omissions in this *Accepted Manuscript* or any consequences arising from the use of any information it contains.

COMMUNICATION

Synthesis of Nitrogen-Doped Carbon Nanostructures from Polyurethane Sponge for Bioimaging and Catalysis

Cite this: DOI: 10.1039/x0xx00000x

Yong Yang, Jingchao Zhang, Jing Zhuang, Xun Wang*

Received 00th January 2012,
Accepted 00th January 2012

DOI: 10.1039/x0xx00000x

www.rsc.org/

A facile and environmentally friendly method to fabricate N-doped carbon nanomaterials was developed by hydrothermal treatment using polyurethane (PU) sponge as a carbon source. We have demonstrated that the hydrothermal decomposition of PU sponge involves a top-down hydrolysis and a bottom-up polymerization for the N-doped carbon dots (N-CDs). Fluorescence property spectroscopy and cytotoxicity studies indicate that these highly-soluble N-CDs show excellent photoluminescent properties and low cytotoxicity, which can be used as good probes for cellular imaging. Besides, N-doped hollow carbon nanostructures can be designed by a simple template method. The prepared N-doped double-shelled hollow carbon nanotubes exhibited excellent ORR electrocatalytic activity and superior durability. Indeed, our results described here can provide an efficient way to synthesize N-doped carbon-based materials for a broad range of applications.

Introduction

Nitrogen doping in carbon-based nanomaterials (N-CMs), including carbon nanotubes,¹ and carbon graphene^{2,3}, show great advantages include supercapacitors,⁴ gas sequestration,⁵ and oxygen reduction reaction.⁶ Up to now, nitrogen heteroatom doping on carbon framework were developed through various methods, including laser irradiation,⁷ electrochemical synthesis,⁸ and pyrolysis.⁹ Nevertheless, these methods always suffer from some drawbacks such as high temperatures, and complicated and time-consuming procedures. In this regard, a facile and low-cost method to synthesize N-CDs is highly desirable.

Recently, functional carbonaceous materials with different sizes and shapes have been intensively studied by hydrothermal carbonization processes using different carbon sources ranging from biomass materials to various synthetic substances¹⁰⁻¹². For example, Zhao and co-workers have demonstrated the hydrothermal preparation of N-doped photoluminescent carbonaceous nanospheres with a quantum yield of ca. 38% for bioimaging.¹³ Sun group synthesized photoluminescent polymer nanodots with grass as the carbon source, which was used as a very effective material for the detection of Cu²⁺.¹⁴ To the best of our knowledge, however, no attention has been paid to preparing N-CMs from commercial PU sponge. Owing to the unique three-dimensional porous structures, PU sponge has always been used as a template to prepare some functional nanocomposites (Fig. S1).¹⁵⁻¹⁶ The corresponding elemental analysis results reveal that carbon and nitrogen account for 55 ~65 wt% and 7 ~8 wt% of the PU sponge, respectively (Table.

S1). Taking nitrogen-rich of PU sponge into consideration, N atoms can be in situ introduced during carbonization process under hydrothermal treatment, which leads to the formation of the N-CMs. More recently, we found that N-doped coating nanocomposites with a controllable thickness can be obtained through the hydrothermal treatment of PU sponge.¹⁷

In this communication, we present a simple, eco-friendly strategy toward N-CMs derived from PU sponge through a green hydrothermal method. The mechanism of hydrothermal decomposition is intensively investigated. We found that this is a generalized carbonization route for PU sponge to synthesize luminescent N-CDs. The resulting highly-soluble N-CDs exhibits low toxicity with excellent biocompatibility for cellular imaging. Most importantly, N-doped hollow carbon nanostructures can be prepared by a simple template method. This strategy can be extended to prepare other nanostructures such as carbon nanocages and carbon fibers. The resulting N-doped double-shelled hollow carbon nanotubes (N-DCTs) demonstrates excellent ORR activities with superior durability and tolerance to methanol crossover. Our results described here not only serve as an efficient way to make better use of PU sponge, but also provide a novel way to synthesize other N-CMs for different applications, such as electrocatalysis and biosensing.

Results and discussion

The hydrothermal treatment of PU sponge at 180 °C generates a yellow dispersion, which is similar to the reported CDs by the hydrothermal route.¹⁸ The morphology of the N-CDs was firstly characterized using transmission electron

microscopy (TEM). As shown in Fig. 1a, the N-CDs are uniform and monodispersed with the size distribution about 2

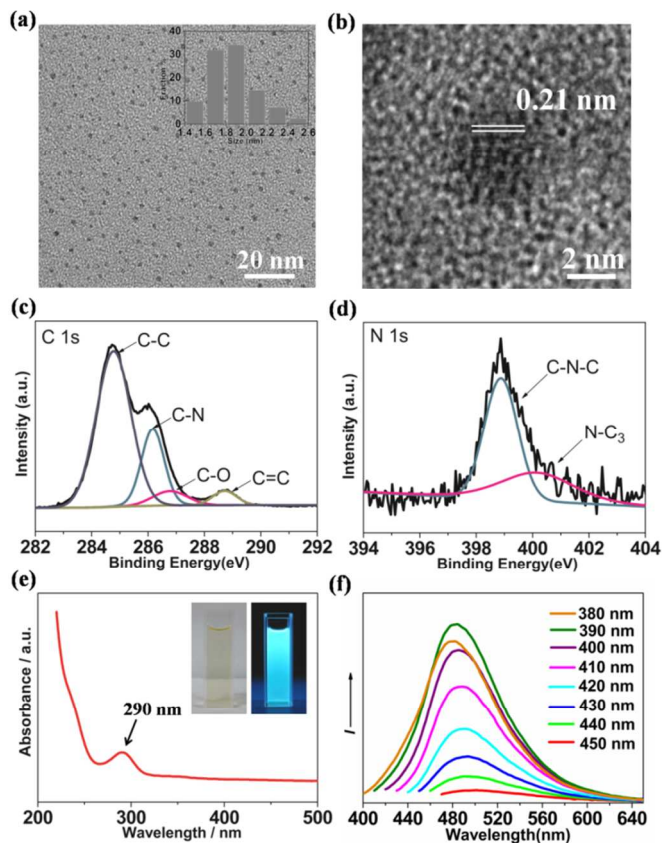


Fig. 1 (a-b) TEM and HRTEM images for as-obtained N-CDs. The insets in (a) is size distribution histogram of N-CDs. (c-d) High-resolution C_{1s} and N_{1s} peaks of as-obtained N-CDs. (e) UV-vis absorption of the N-CDs solution in. Photograph of the aqueous solution of the N-CDs solution in water excited by daylight and UV irradiation (365 nm). (f) Photoluminescence emission spectra of the N-CDs excited at different excitation wavelengths.

nm. The structures of the N-CDs were characterized by atomic force microscopy (AFM, Fig.S2) and the topographic heights of N-CDs were about 1 nm. The high-resolution TEM (HRTEM) image (Fig. 1b) clearly reveals that the as-synthesized N-CDs possess a crystalline structure with lattice spacing of 0.203 nm, which agrees well with the (110) lattice spacing of sp^2 graphitic carbon.^{7,18a}

X-ray photoelectron spectroscopy (XPS) was further used to analyze the composition of the as-produced N-CDs. The survey spectrum (Fig.S3) of the N-CDs shows three typical peaks of C_{1s} , N_{1s} , and O_{1s} . The C_{1s} spectrum (Fig. 1c) shows four peaks at 284.8, 286.1, 286.7, and 288.7 eV, which are assigned to C-C, C-N, C-O, and C=N/C=O, respectively.¹⁹ The high-resolution N_{1s} spectrum (Fig. 2d) reveals the presence of C-N-C (398.7 eV), and N-C₃ (399.2 eV).²⁰ In Fourier transform infrared spectra (Fig.S4), the broad peak centered at 3430 cm^{-1} was assigned to O-H or N-H vibrations; the strong peak at 1636 cm^{-1} was designated to C=O vibrations. The stretching vibrations of N-related bonds and C-NH-C were exhibited by the peaks at 1384 and 1106 cm^{-1} . These results are in agreement with the XPS results. The XPS results (Table S3) also show that

the N-CDs have high oxygen content (21.72%), suggesting a low graphitic level for the N-CDs. These results reveal that these N-CDs were rich in oxygen (hydroxyl, carbonyl, or carboxylic acid groups) and nitrogen containing functional groups derived from the dehydration and polymerization of PU sponge.

Fig. 1e shows an absorption band at ca. 290 nm, which is familiar with previous reported CDs due to the $p-p^*$ transition of aromatic sp^2 domains.^{21,22} The yellow dispersion was found to emit intense blue color under 365 nm UV light (insets in Fig. 1d). Different excitation wavelengths were carried out to investigate the fluorescent properties of the as-prepared N-CDs. As shown in Fig. 1f, when the excitation wavelength changes from 380 to 450 nm (10 nm interval), the intensity decrease gradually and the PL peak correspondingly shifts from 480 nm (orange) to 490 nm (red). The fluorescence of the N-CDs is dependent on the excitation wavelength, which is ascribed to the different emissive trap sites of the CDs and the size distribution of the CDs.^{23,24} When N-CDs were excited at 390 nm, the most intense emission wavelength was about 480 nm. The as-prepared N-CDs solution can remain homogeneous for several months storage without any changes. Impressively, it was found that the hydrothermal treatment of a series of commercial PU sponges also leads to a yellow solution in the same reaction conditions and the corresponding dispersion shows the same blue color under UV light (Table S2), indicating that these dispersion have the similar fluorescent property. Therefore, we believe that this is a generalized carbonization route for PU sponge during the hydrothermal process.

We found that N-doped carbon spheres (N-CSs) can be synthesized in higher concentrations at higher temperatures without any additives. As shown in Fig. S5, the N-CSs are uniform and spherical with average diameters of 300 nm. Elemental mapping shows that the elements C, N, and O are homogeneously distributed in the whole nanoparticles. The nitrogen-to-carbon signal ratio of 0.11 is similar to that of pristine PU sponge (0.118), implying that the N-CSs are derived from the carbonization of PU sponge. Compared with PU sponge, there was an increase in carbon content and decrease in oxygen content, which is consistent with an aromatization and carbonization process described in the van Krevelen diagram.^{25,26} To gain insight into the mechanism of hydrothermal decomposition of PU sponges, time-dependent experiments were carried out by TEM as shown in Fig. S6. After hydrothermal treatment at 200°C for 1 h, a yellow dispersion was obtained, which indicates that PU sponge decomposed into monomers. As the reaction proceeds, it was found that the colour of the solution gradually changed into brown due to the rising N-CSs concentration. The process of carbonization at higher reaction temperatures with longer reaction time was favourable and the diameter of the N-CSs and the yields increased, as confirmed by TEM. This is similar to the previous well-known hydrothermal carbonization process of carbohydrates. Based on above results, we propose that the formation of N-doped carbon material undergoes the consequence of polymerization and carbonization. Initially, PU sponge was decomposed into some monomers through a top-down hydrolysis during the initial hydrothermal stage. With the increase of reaction time, these monomers may assemble into polymeric intermediates via a polymerization and carbonization, leading to N-doped carbonaceous materials.

Interestingly, N-doped hollow carbon structure can be prepared by a simple template method. The schematic synthesis of the N-doped double-shelled hollow carbon nanotubes (N-DCTs) is shown in Fig. 2a. This strategy involves the hydrothermal synthesis of MnO_2 @N-Cs composites, followed by carbonization to obtain N-doped carbon encapsulated MnO_2 nanotubes, and finally acid etching of MnO_2 template. MnO_2 coated by N-doped carbonaceous layer were synthesized by using PU sponges as carbon source via a hydrothermal method (see Experimental section). As shown in Fig. S7, MnO_2 nanotubes were uniformly coated by a carbonaceous layer.

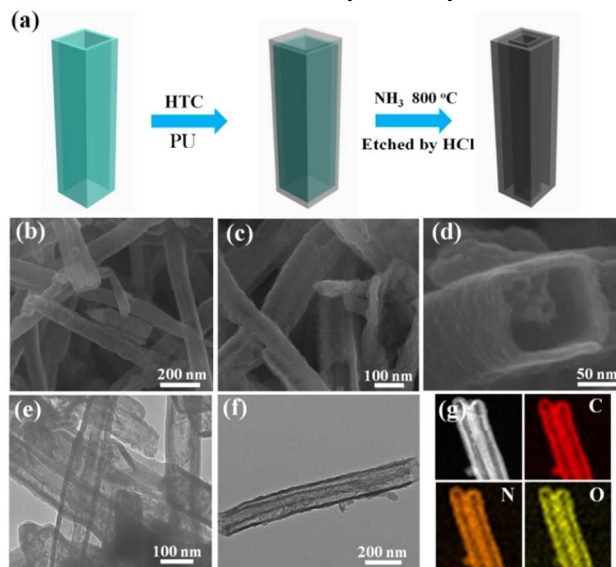


Fig. 2 (a) Schematic illustration of the formation process of the N-DCTs. (b-d) SEM images of N-DCTs under different magnifications, displaying the tube-in-tube carbon nanostructure. (e-f) TEM images of N-doped carbon nanofibers. (g) HAADF-STEM image and the corresponding EDS mapping images, indicating that C, N and O are uniformly distributed in this architecture.

Then, the as-prepared MnO_2 @N-Cs composites were further treated by high temperature calcinations under NH_3 atmosphere, resulting in the carbonization of the coating layer.²⁷ After removing manganic oxide by acid etching, N-doped carbon nanostructure with tube in tube can be obtained. Fig. 2b shows SEM image of the as-obtained N-doped carbon nanotubes. A typical broken hollow nanotube shown in Fig. 2c confirmed that the hollow interior structure. It should be emphasized here that the obvious tube-in-tube carbon nanostructure is observed from the high magnification SEM and TEM images (Fig. 2d). The as-obtained N-DCTs are highly uniform with a diameter of 100 nm and a length of 1–2 μm . The thickness of the carbon layer was estimated to be about 10 nm. The tube-in-tube carbon nanostructure with large internal void space can be attributable to the etching of MnO_2 tubular structure (Fig. 2e). In addition, EDS elemental mapping shows that the elements C, N and O are distributed throughout the whole nanotubes (Fig. 2g), suggesting that nitrogen has successfully doped in carbon skeleton. X-ray diffraction (XRD) pattern of N-CNTs (Fig. S8) shows two characteristic peaks located at about 25° and 43° , which can be indexed to the (002) and (100) planes of graphite. The corresponding Raman spectrum shows that there are two broad bands located at 1348 and 1583 cm^{-1} , which belong to the D band and G band, respectively. The XPS results (Fig. S9) show that the N-

CSs are composed of C (81.83%), O (11.04%) and N (7.13%) atoms. What is more, XPS results also indicate that there is no peak of Mn after acid etching, indicating no metal residue in the final products. Such nitrogen-rich nanotubes with double-shelled structure could be useful in electrocatalytic applications.

This template strategy could be extended to design other N-doped carbon nanostructures by changing various templates. For example, N-doped carbon nanocages and nanofibers can be obtained by using Mn_3O_4 octahedrons and MnO_2 nanowires through the same template method. The morphology and structural features of as-prepared N-doped carbon nanocages were characterized by SEM and TEM. Fig. 3a shows SEM image of the as-obtained N-doped hollow carbon octahedron, which exhibits well-defined polyhedral structure with diameters of 200–300 nm. From a broken nanocage as shown in Fig. 3b, the hollow interior can be clearly observed. As shown in Fig. 3d–e, the structure of octahedron can be well retained and duplicated. The corresponding selected area electron diffraction (SAED) pattern (Fig. 3f) shows the amorphous feature of the N-doped hollow carbon nanocages. For N-doped carbon nanofibers, MnO_2 nanowires can also be fully covered with cable-like structure (Fig. 3g–h). Note that obvious hollow interior structure can be seen in the middle of fiber structure after etching (Fig. 3i). To better understand the evolution process of Mn_3O_4 @N-Cs composites, time-dependent experiments were investigated by TEM analysis. As shown in Fig. S10, Mn_3O_4 octahedrons were fully coated with a uniform layer derived from PU sponges, displaying a well-defined core-shell structure. As reaction proceeds, it was obvious to see that some Mn_3O_4 octahedrons gradually dissolve during the hydrothermal treatment, which may be ascribed to the dissolution of template in acid solution derived from the carbonization of PU sponge. A continuous evolution from core-shell structures to hollow structure could be observed under different hydrothermal stages. Nitrogen adsorption–desorption isotherms and pore size distribution measurements was measured to examine the the porous structure of carbon nanocages, the Brunauer-Emmett-Teller (BET) specific surface area of the as-prepared nanocages is $97.3\text{ m}^2\text{ g}^{-1}$ with the existence of micropores (Fig. S10).

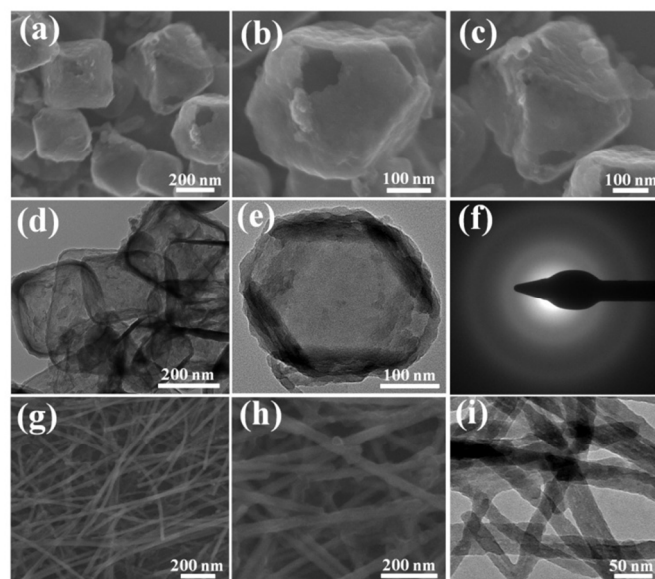


Fig. 3 (a-b) SEM images of N-doped carbon nanocages. (d-e) TEM and HRTEM images of N-doped carbon nanocages. (f) SAED pattern of N-doped carbon nanocages. (g-h) SEM images of MoO₂@N-Cs under different magnifications. (i) TEM images of N-doped carbon nanofibers.

To evaluate the cytotoxicity of N-CDs, MKN-45 cells and hela cells were cultured after being exposed to N-CDs at different concentrations to evaluate the relative cell viability through MTT assays.¹³ As shown in Fig. S12, the cell viabilities of MKN-45 cells and hela cells retained over 80% viability even in the presence of 160 $\mu\text{g mL}^{-1}$ N-CNs, implying that the N-CNs has low cytotoxicity and good biocompatibility. For confocal microscopic imaging, the N-CDs labeled cells were further used to study its intracellular fluorescence by a confocal microscopy. It was found that MKN-45 and Hela cells incubated with N-CDs showed bright blue light under the excitation of 405 nm (Fig. 5). The fluorescence images show that the N-CDs could easily translocate into the cytoplasm of cells. Moreover, it can be seen that the cell membrane can be well labeled and the cell nucleus is very weak, suggesting that very few N-CDs

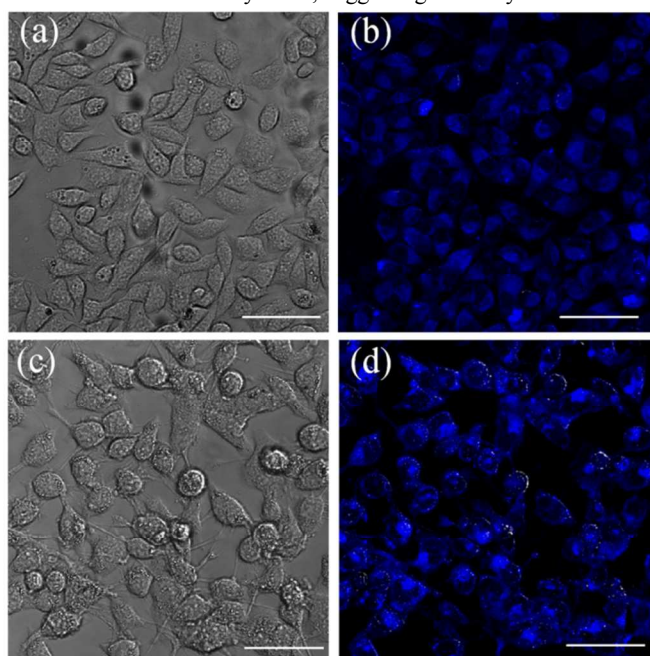


Fig. 4 Images of N-CDs incubated MKN-45 cells obtained under bright field (a) and excitation wavelength (b). Images of N-CDs incubated hela cells obtained under bright field (c) and excitation wavelength (d). The samples were excited at 405 nm. All scale bars: 50 μm .

enter the inner nuclei. Owing to the low cytotoxicity and excellent biocompatibility, these fluorescent N-CDs can be used as a good bioimaging material.

The as-synthesized N-DCTs were tested as metal-free catalysts for ORR in electrochemistry. As shown in Fig. 5a, there is no significant peak in the N₂-saturated KOH solution. In contrast, a distinct reduction peak can be observed in the O₂-saturated solution. Notably, the resulting N-DCTs exhibit a big cathodic current density with low onset potentials, which indicates the prominent ORR performance of N-DCTs. RDE voltammetry measurements under different rotation rates were carried out to calculate the number of the electron transfer per oxygen molecule, as shown in Fig. 5b. The current density increases with an increased in rotation rate because

of the enhanced diffusion of electrolytes. The transferred electron number can be calculated using the Koutecky–Levich equation and the corresponding curves are plotted for different potentials (Fig. 5c).²⁸ It can be seen that the K–L plots (j^{-1} vs $\omega^{-1/2}$) have good linearity at various potentials from -0.4V to -0.7 and the electron transfer number (n) was 3.87 at -0.4 V, which is close to the one-step, four-electron pathway for ORR. Rotation ring disk electrode (RRDE) studies were further carried out to acquire the ORR pathway by monitoring the intermediate peroxide species of HO₂⁻ generated at the disk electrode in an alkaline medium. As shown in Figure 5d, the electron-transfer numbers (n) were measured over the potential range of -0.2 to -0.7 V to be 3.64–3.86 for N-DCTs, which is consistent with the RDE result.

Chronoamperometric responses were further used to verify the remarkable electrocatalytic performances of as-obtained N-DCTs. As shown in Fig. 5e, a drastic response was found for the Pt/C catalyst when 3 mL of methanol was added. However, no distinct decrease in the cathodic current was observed for DCTs electrode, indicating that the DCTs have a stronger tolerance to the methanol crossover effect. In addition, the durability of the N-DCTs for ORR was evaluated by a chronoamperometric approach (Fig. 5f). The N-DCTs exhibited only slight degradation after 10000 s, whereas, the corresponding current loss for the commercial Pt/C decreased about 20% under the same conditions, suggesting that the DCTs is much more stable than the Pt/C electrode. The outstanding ORR activity of N-DCTs could be ascribed to the unique double-shelled hollow structure and the high content of pyridine and pyrrolic nitrogen after annealing in NH₃ atmosphere. In short, the N-DCTs derived from PU sponge show promising application as metal free electrocatalysts.

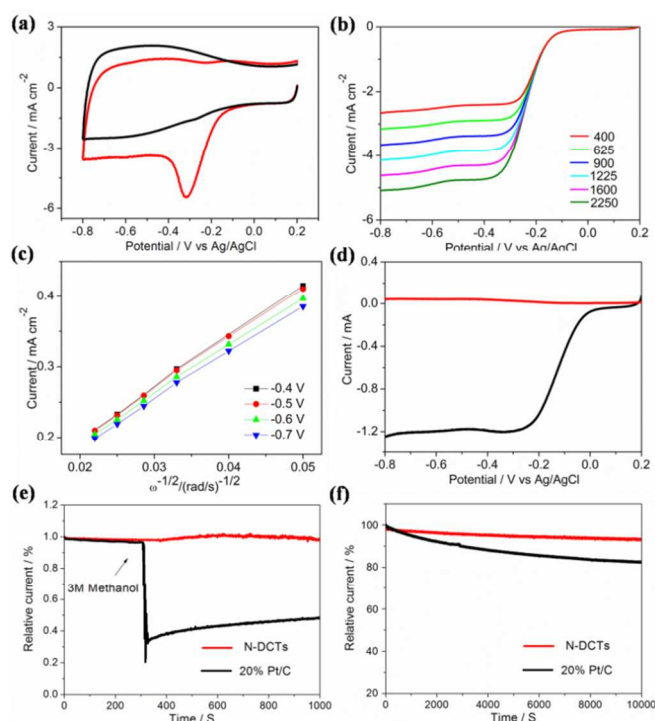


Fig. 5 (a) Cyclic voltammetry of the N-DCTs performed on a GC electrode in O₂-saturated (red) and N₂-saturated (black) at a scan rate of 100 mV/s; (b) ORR curves of N-DCTs in O₂-saturated 0.1 M KOH at scan rate of 10 mV/s with different speeds. (c) Koutecky–Levich plots of j^{-1} versus $\omega^{-1/2}$ obtained from the RDE data at different electrode potentials. (d) RRDE voltammograms of N-DCSS in O₂-saturated 0.1 M KOH at 1600 rpm. Chronoamperometric response for ORR at N-DCSSs and Pt/C electrodes: (e) on addition of 3 mL of methanol; (f) Durability evaluation of N-DCSSs and Pt/C electrodes for 10,000 s at -0.4 V and a rotation rate of 900 rpm.

Conclusions

In summary, we have demonstrated a green strategy to synthesize N-CDs and N-DCTs through hydrothermal treatment of commercial PU sponge for the first time. We have demonstrated that the hydrothermal decomposition of PU sponge involves a top-down hydrolysis and a bottom-up polymerization. These highly-soluble N-CDs possess excellent cytocompatibility and can be successfully used in imaging living cells. Moreover, N-doped hollow carbon nanostructures can be designed through a simple template strategy. The resulting N-DCTs exhibited excellent ORR electrocatalytic activity with better tolerance to the methanol crossover effect and superior durability over that of the Pt/C electrode. And it makes our method doubly attractive that it is a low-cost and eco-friendly one, which will be helpful in recycling PU sponge and can be applied as an efficient technology to prepare N-doped carbon-based materials for various applications in energy storage and electrocatalysis.

Acknowledgements

This work was supported by NSFC (91127040, 21221062), and the State Key Project of Fundamental Research for Nanoscience and Nanotechnology (2011CB932402).

Experimental section

Chemicals: All chemicals were purchased from Sinopharm Chemical Reagent Beijing Company and were used as received without further purification. Deionized water was used throughout the experiment.

Hydrothermal synthesis of N-CDs from PU sponges: For the fluorescent N-CDs, the as-prepared PU sponge (30mg) was immersed into 30 ml of distilled water, then added into a 50 mL Teflon-lined autoclave and heated at 180 °C for several hours. After the reaction completed, the autoclave was cooled down naturally. Next, the faint yellow upper aqueous solution was collected by removing the insoluble materials through simple filtration.

Synthesis of MnO₂ nanotubes: The MnO₂ nanotubes were synthesized using the reported method. In a typical procedure, KMnO₄ (0.4g) and HCl (5 ml, 1M) were added to 30 mL deionized water under intense stirring and transferred to a Teflon vessel held in a stainless steel vessel. The autoclave was sealed and hydrothermally treated at 140 °C for 12 h. After cooling, the black precipitates were collected by centrifugation and washed by deionized water to remove possible impurities or excess ions.

Synthesis of Mn₃O₄ octahedrons: The Mn₃O₄ octahedrons were synthesized using a hydrothermal method described previously. Typically, KMnO₄ (0.1g) was dissolved into 20 mL of 10 g/L CMC

under intense stirring and transferred to a Teflon vessel held in a stainless steel vessel. The sealed vessel was placed in an oven and heated at 140°C for 6h. After cooling, the yellow product was washed several times and finally dried in air.

Synthesis of MnO₂ nanowires: The MnO₂ nanowires were synthesized using a hydrothermal method described previously. Briefly, 0.1 g of MnSO₄·H₂O, 20 mL of (NH₄)₂S₂O₈ and ammonium sulfate (NH₄)₂SO₄ was added into 36 ml of distilled water under intense stirring. Then the mixture was transferred and sealed in a 50 mL Teflon-lined autoclave, heated at 180 °C for 12 h, and finally cooled to room temperature. The black precipitate was collected by centrifugation, washed alternately with deionized water and ethanol four times, and dried in air.

Preparation of N-DCTs

Typically, a certain amount of MnO₂ nanotubes were dissolved in 30 mL of water. Then, the prepared PU sponge was added. The solution was transferred to a 50 mL Teflon-lined stainless steel autoclave and sealed. The autoclave was then heated at 200°C for 8 h. After cooling, the product was collected by removing the insoluble materials through simple filtration. Finally, the product was harvested by centrifugation. The as-synthesized MnO₂ nanotubes with N-doped carbon coating samples was placed into a horizontal furnace and heated to 800 °C for 3 h with a heat rate of 5 °C min⁻¹ in NH₃. Finally, the N-doped carbon nanotubes was washed with HCl to remove the MnO₂ templates and other impurities, washed with deionized water several times and finally dried in air.

Cell Culture and MTT Assay

The cytotoxicity of the N-CDs was tested on MKN-45 cells and hela by 3-(4, 5-dimethylthiazol-2-yl)-2, 5-diphenyltetrazolium bromide (MTT) assay. Briefly, the cells were cultured in Dulbecco's Modified Eagle Medium (DMEM, HyClone) with high glucose, containing 10% fetal bovine serum (FBS), 100 U·mL⁻¹ penicillin and 100 mg·mL⁻¹ streptomycin at 37 °C in 5% CO₂ humidified atmosphere. Then, cells were seeded in a glass bottom dish at a density of approximately 3×10³ cells per well in a 96-well plate. Cells were subsequently incubated at 37 °C in a 5 % of CO₂ humid incubator for 24 h. The following morning, the N-CDs were added to the cells with increasing concentrations at 10, 20, 40, 80, and 160 µg mL⁻¹, respectively. Cells were then incubated for 24 h at 37 °C. Afterward, the medium containing N-CDs was removed, and replaced with 200 µL fresh medium containing 20 µL MTT (5 mg/ml in PBS) and incubated for another 4 h. Finally all medium was removed and 150 µL/well DMSO was added, followed by shaking for 15 min. The absorbance of each well was measured at 570 nm using in a Multiskan MK3 microplate photometer (Thermo Scientific, USA) with pure DMSO as a blank. Cells cultured with the pure culture medium were set as controls. The relative cell viability was expressed as mean ± standard deviation (SD).

Confocal microscopic imaging

For confocal microscopy, cells were seeded on a coverslip in 6-well plate before use. At the day before imaging, cells were transferred and plated on a 35-mm Petri dish in DMEM one day in advance for cell imaging. For cell imaging studies, cells were incubated in DMEM containing 0.08 mg mL⁻¹ of N-CDs for 2 hours at 37 °C, The cells were then washed with isotonic PBS (pH 7.4) three times to remove the extracellular remaining N-CDs. The samples were examined under a confocal laser scanning microscope (Nikon A1) equipped with an Ar laser (405nm).

ORR measurement

A standard three-electrode configuration was used for the cyclic voltammetry (CV) measurements on a CHI 760D potentiostat at a scan rate of 100 mV/s. For all electrochemical measurements, an aqueous solution of 0.1 M KOH was used as the electrolyte. N₂ or

O₂ was used to purge the solution to achieve the N₂⁻ or O₂⁻ saturated 0.1M KOH solution at room temperature. A Pt plate and Ag/AgCl were used as counter and reference electrodes, respectively. RDE or RRDE voltammetry was performed on a MSR-X electrode rotator (Pine Instrument) and the CHI 760D potentiostat at a scan rate of 10 mV/s.

Characterization

The morphology and size of the nanostructures were characterized by a HITACHI H-7700 TEM with an accelerating voltage of 100 kV, and a FEI Tecnai G2 F20 S-Twin high-resolution (HR) TEM equipped with energy dispersive spectrometer (EDS) analyses at 200 KV. The scanning electron microscope (SEM) was performed on a LEO 1530. The crystal structure was analyzed by a Bruker D8-advance X-ray powder diffractometer operated at 40 kV voltage and 40 mA current with CuK α radiation ($\lambda=1.5406 \text{ \AA}$). IR spectra were measured by using a Perkin Elmer FTIR spectrophotometer on KBr pellets in the range of 4000-400 cm⁻¹ with the resolution of 4 cm⁻¹. Elemental analysis of C, H, and N was carried out on a VarioEL (ElementarAnalysensysteme GmbH). Atomic force microscopic (AFM) images were carried out by the use of a Nanoscope III MultiMode SPM (Digital Instruments, U.S.A.) with an AS-12 ("E") scanner operated in tapping mode in conjunction with a V-shaped tapping tip (Applied Nanostructures SPM model: ACTA). X-ray photoelectron spectroscopy (XPS) experiments were carried out on scanning X-ray microprobe (Quantera SXM, ULVAC-PHI. INC) operated at 250 kV, 55 eV with monochromated Al K α radiation. The fluorescent images were taken by using a fluorescent microscopy Nikon A1. Photoluminescence (PL) emission measurements were performed by a LS 55 fluorescence spectrometer (PerkinElmer). Raman spectra were recorded using a HORIBA JY HR800 confocal microscope Raman spectrometer employing an Ar-ion laser operating at 633 nm.

References

1. K. P. Gong, F. Du, Z. H. Xia, M. Durstock, L. M. Dai, *Science*, 2009, **323**, 760-764.
2. J. Liang, Y. Jiao, M. Jaroniec, S. Z. Qiao, *Angew. Chem. Int. Ed.*, 2012, **51**, 11496-11500.
3. W. Zhou, X. Xiao, M. Cai, L. Yang, *Nano Lett.*, 2014, **14**, 5250-5256.
4. (a) W. Li, F. Zhang, Y. Q. Dou, Z. X. Wu, H. J. Liu, X. F. Qian, D. Gu, Y. Y. Xia, B. Tu, D. Y. Zhao, *Adv. Energy Mater.*, 2011, **1**, 382-386; (b) K. Zhang, Z. Hu, Z. L. Tao, J. Chen, *Sci China Mater*, 2014, **1**, 42-58.
5. J. Wei, D. D. Zhou, Z. K. Sun, Y. H. Deng, Y. Y. Xia, D. Y. Zhao, *Adv. Funct. Mater.*, 2013, **23**, 2322-2328.
6. (a) Y. G. Li, W. Zhou, H. L. Wang, L. M. Xie, Y. Y. Liang, F. Wei, J. C. Idrobo, S. J. Pennycook, H. J. Dai, *Nat. Nano.*, 2013, **7**, 394-400; (b) Y. Li, Y. Zhao, H. H. Cheng, Y. Hu, G. Q. Shi, L. M. Dai, L. T. Qu, *J. Am. Chem. Soc.*, 2011, **134**, 15-18; (c) C. L. Han, S. P. Wang, J. Wang, M. M. Li, J. Deng, H. R. Li, Y. Wang, *Nano Res*, 2013, **12**, 1809-1819; (d) Z. Y. Liu, G. X. Zhang, Z. Y. Lu, X. Y. Jin, Z. Chang, X. M. Sun, *Nano Res*, 2013, **4**, 293-301.
7. S. L. Hu, K. Y. Niu, J. Sun, J. Yang, N. Y. Zhao, X. W. Du, *J. Mater. Chem.*, 2009, **19**, 484-488.
8. J. Zhou, C. Booker, R. Li, X. Zhou, T. Sham, X. Sun, Z. Ding, *J. Am. Chem. Soc.*, 2007, **129**, 744-745.
9. H. P. Liu, T. Ye, C. D. Mao, *Angew. Chem. Int. Ed.*, 2017, **119**, 6593-6595.
10. (a) C. Zhu, J. Zhai, S. Dong, *Chem. Commun.*, 2012, **75**, 9367-9369; (b) D. Kim, Y. Choi, E. Shin, Y.K. Jung, B. Kim, *RSC Advances.*, 2014, **12**, 23210-6595; (c) Z. Zhang, J. H. Hao, J. Zhang, B. L. Zhang, J. L. Tang, *RSC Advances.*, 2012, **2**, 8599-8601.
11. (a) Y. Hu, J. Yang, J. Tian, L. Jia, J. Yu, *RSC Advances.*, 2014, **4**, 47169-47176; (b) S. Sahu, B. Behera, T.K. Maiti, S. Mohapatra, *Chem. Commun.*, 2012, **48**, 88358837; (c) J. Wei, J. Shen, X. Zhang, S. Guo, J. Pan, X. Hou, H. Zhang, L. Wang, B. Feng, *RSC Advances.*, 2013, **3**, 13119-13122.
12. (a) H. Huang, J. Lv, D. Zhou, N. Bao, Y. Xu, A. Wang, J. Feng, *RSC Advances.*, 2013, **3**, 21691-21696; (b) B. Chen, F. Li, S. Li, W. Weng, H. Guo, T. Guo, X. Zhang, Y. Chen, T. Huang, X. Hong, S. You, Y. Lin, K. Zeng, S. Chen, *Nanoscale*, 2013, **5**, 1967-1971.
13. W. Li, Z. H. Zhang, B. Kong, S. S. Feng, J. X. Wang, L. Z. Wang, J. P. Yang, F. Zhang, P. Y. Wu, D. Y. Zhao, *Angew. Chem. Int. Ed.*, 2013, **52**, 8151-8155.
14. S. Liu, J. Q. Tian, L. Wang, Y. W. Zhang, X. Y. Qin, Y. L. Luo, A. M. Asiri, A. O. Al-Youbi, X. P. Sun, *Adv. Mater.*, 2012, **24**, 2037-2041.
15. (a) W. Chen, R. B. Rakhi, L. B. Hu, X. Xie, Y. Cui, H. N. Alshareef, *Nano Lett.*, 2011, **11**, 5165-5172; (b) C. Wu, X. Y. Huang, X. F. Wu, R. Qian, P. K. Jiang, *Adv. Mater.*, 2013, **25**, 5658-5662; (c) J. Ge, H. B. Yao, X. Wang, Y. D. Ye, J. L. Wang, Z. Y. Wu, J. W. Liu, F. J. Fan, H. L. Gao, C. L. Zhang, S. H. Yu, *Angew. Chem. Int. Ed.*, 2013, **52**, 1654-1659.
16. (a) H. B. Yao, J. Ge, C. F. Wang, X. Wang, H. Hu, Z. J. Zheng, Y. Ni, S. H. Yu, *Adv. Mater.*, 2013, **25**, 6692-6998; (b) B. Kong, J. Tang, Z. X. Wu, J. Wei, H. Wu, Y. C. Wang, G. F. Zheng, D. Y. Zhao, *Angew. Chem. Int. Ed.*, 2014, **53**, 2888-2892.
17. Y. Yang, J. C. Zhang, S. T. Wang, X. B. Xu, Z. C. Zhang, P. P. Wang, Z. L. Tang, X. Wang, *Nanoscale*, 2015, **7**, 3254-3262.
18. (a) J. Wang, F. Peng, Y. Lu, Y. Zhong, S. Wang, M. Xu, X. Ji, Y. Su, L. Liao, Y. He, *Adv. Opt. Mater.*, 2015, **3**, 103-111; (b) Q. N. Meng, L. Wang, J. H. Zhang, Y. B. Song, H. Jin, K. Zhang, H. C. Sun, H. Y. Wang, B. Yang, *Angew. Chem. Int. Ed.*, 2013, **52**, 3953-3957. (c) Y. B. Song, S. J. Zhu, B. Yang, *RSC Advances.*, 2014, **4**, 27184-27200.
19. C. H. Zhang, L. Fu, N. Liu, M. H. Liu, Y. Y. Wang, Z. F. Liu, *Adv. Mater.*, 2011, **23**, 1020-1024.
20. W. Ai, Z. M Luo, J. Jiang, J. H. Zhu, Z. Z. Du, Z. X. Fan, L. H. Xie, H. Zhang, W. Huang, T. Yu, *Adv. Mater.*, 2014, **26**, 6186-6192.
21. A. Jaiswal, S.S. Ghosh, A. Chattopadhyay, *Chem. Commun.*, 2012, **48**, 407-409.
22. Q. Hu, M.C. Paau, Y. Zhang, X. Gong, L. Zhang, D. Lu, Y. Liu, Q. Liu, J. Yao, M.M.F. Choi, *RSC Advances.*, 2014, **4**, 18065-18073.
23. Z. T. Fan, S. H. Li, F. L. Yuan, L. Z. Fan, *RSC Advances.*, DOI: 10.1039/C4RA17131D.
24. Y. Fang, S. Guo, D. Li, C. Zhu, W. Ren, S. Dong, E. Wang, *ACS Nano*, 2012, **6**, 400-409.
25. D. W. Van Krevelen, *Fuel*, 1950, **29**, 269-284.
26. M. Sevilla, A.B. Fuertes, *Chem. Eur. J.*, 2009, **15**, 4195-4203.

Journal Name

27. P. Chen, L. Wang, G. Wang, M. Gao, J. Ge, W. Yuan, Y. Shen, A. Xie, S. Yu, *Energy Environ. Sci.* 2014, **7**, 4095-4103.
28. S. Wang, D. Yu, L. Dai, *J. Am. Chem. Soc.* 2011, **133**, 5182-5185.

TOC

